MIT Open Access Articles

A CHANDRA OBSERVATION OF THE BURSTING MILLISECOND X-RAY PULSAR IGR J17511–3057

The MIT Faculty has made this article openly available. *Please share* how this access benefits you. Your story matters.

Massachusetts Institute of Technology

A *CHANDRA* OBSERVATION OF THE BURSTING MILLISECOND X-RAY PULSAR IGR J17511−3057

A. PAIZIS[1], M. A. NOWAK[2], J. RODRIGUEZ[3], J. WILMS[4], S. CHATY[3], M. DEL SANTO[5], AND P. UBERTINI[5]

[1] Istituto Nazionale di Astrofisica, INAF-IASF, Via Bassini 15, 20133 Milano, Italy; ada@iasf-milano.inaf.it
[2] Massachusetts Institute of Technology, Kavli Institute for Astrophysics, Cambridge, MA 02139, USA; mnowak@space.mit.edu
[3] Astrophysique, Instrumentation et Modélisation (AIM, UMR-E 9005 CEA/DSM-CNRS-Université Paris Diderot) Irfu/Service d'Astrophysique,
Centre de Saclay, F-91191 Gif-sur-Yvette Cedex, France
[4] Dr. Karl Remeis-Sternwarte and Erlangen Centre for Astroparticle Physics, Universität Erlangen-Nürnberg, Sternwartstr. 7, 96049 Bamberg, Germany
[5] IAPS, INAF, Via Fosso del Cavaliere 100, 00133 Rome, Italy

ABSTRACT

IGR J17511−3057 is a low-mass X-ray binary hosting a neutron star and is one of the few accreting millisecond X-ray pulsars with X-ray bursts. We report on a 20 ks *Chandra* grating observation of IGR J17511−3057, performed on 2009 September 22. We determine the most accurate X-ray position of IGR J17511−3057, $\alpha_{J2000} = 17^h51^m08^s.66$, $\delta_{J2000} = -30°57'41''.0$ (90% uncertainty of $0''.6$). During the observation, a $\sim$54 s long type-I X-ray burst is detected. The persistent (non-burst) emission has an absorbed 0.5–8 keV luminosity of 1.7×10^{36} erg s^{-1} (at 6.9 kpc) and can be well described by a thermal Comptonization model of soft, $\sim$0.6 keV, seed photons upscattered by a hot corona. The type-I X-ray burst spectrum, with average luminosity over the 54 s duration $L_{0.5-8\,keV} = 1.6 \times 10^{37}$ erg s^{-1}, can be well described by a blackbody with $kT_{bb} \sim 1.6$ keV and $R_{bb} \sim 5$ km. While an evolution in temperature of the blackbody can be appreciated throughout the burst (average peak $kT_{bb} = 2.5^{+0.8}_{-0.4}$ keV to tail $kT_{bb} = 1.3^{+0.2}_{-0.1}$ keV), the relative emitting surface shows no evolution. The overall persistent and type-I burst properties observed during the *Chandra* observation are consistent with what was previously reported during the 2009 outburst of IGR J17511−3057.

Key words: accretion, accretion disks – pulsars: individual (IGR J17511-3057) – stars: neutron – X-rays: binaries – X-rays: bursts

Online-only material: color figures

1. INTRODUCTION

Low-mass X-ray binaries containing a neutron star (hereafter NS LMXBs) are very old systems (10^8–10^9 yr), with an NS magnetic field that is believed to have decayed to about 10^8–10^9 G. It is believed that since the NS spends a substantial fraction of its life accreting gas via an accretion disk, it is finally spun-up to millisecond levels (Tauris & van den Heuvel 2006). This belief is supported by the fact that in 23 cases (out of more than 150 known LMXBs; Liu et al. 2007) the NS spin frequency has been detected at the millisecond level (see Patruno 2010, for a complete list). These detections support the scenario that LMXBs are the progenitors of millisecond radio pulsars with a low magnetic field.

When pulsations occur during surface thermonuclear explosions, known as type-I X-ray bursts (see Strohmayer & Bildsten 2006, for a review), the sources are known as *nuclear powered X-ray pulsars* (hereafter NPXP). Up to now, pulsations during bursts (called burst oscillations) have been detected in 15 sources (Altamirano et al. 2010). During these events, the accumulated nuclear fuel first ignites at the point of the NS surface where it reaches the critical ignition column density and then spreads to all adjacent areas on the surface. When nuclear burning occurs uniformly over the surface, no "hot spot" is created and the NS spin will still be hidden. But in some cases a "patchy" burning process can occur, making the NS spin period visible. With the decrease of the X-ray burst flux, the non-uniformity fades out and so do the pulsations.

In other cases, pulsations occur in the "persistent" X-ray emission (i.e., not during type-I X-ray bursts), and the sources are known as *accreting millisecond X-ray pulsars* (hereafter AMXP). Up to now, 14 such sources have been detected (all

transient X-ray sources; Patruno & Watts 2012; Papitto et al. 2011) and it is believed that matter from the accretion disk is channeled by the magnetic field lines onto the magnetic poles, forming a hot spot visible in X-rays. An important detection for our comprehension of the pulsating mechanism in AMXPs (versus the non-pulsating majority of LMXBs) was achieved with the discovery of pulsations that were not detected throughout the outburst, but only intermittently, e.g., as in HETE J1900.1−2455 (Kaaret et al. 2006), Aql X-1 (Casella et al. 2008), and SAX J1748.9−2021 (Altamirano et al. 2008). These sources are important because they may be the intermediate link between persistent AMXPs and non-pulsating NS LMXBs.

Of the currently known 14 AMXPs, only five, including IGR J17511−3057, belong to both the NPXP and AMXP classes, i.e., show pulsations during type-I X-ray bursts *and* during the persistent (non-burst) emission (Altamirano et al. 2010).

On 2009 September 12 (MJD 55087) *INTEGRAL* discovered a new hard X-ray source, IGR J17511−3057 (Baldovin et al. 2009), detected during the *INTEGRAL* Galactic bulge monitoring program (Kuulkers et al. 2007). Shortly thereafter, we reported the best X-ray position of the source from a preliminary analysis of our *Chandra* data: $\alpha_{J2000} = 17^h51^m08^s.66$, $\delta_{J2000} = -30°57'41''.0$ (90% uncertainty of $0''.6$; Nowak et al. 2009). Near-infrared follow-up observations identified within the *Chandra* error box the counterpart at a magnitude of $K_s = 18.0 \pm 0.1$ (Torres et al. 2009a, 2009b), but no radio counterpart was detected with a 3σ upper limit of 0.10 mJy (Miller-Jones et al. 2009).

Shortly after the discovery, pulsations at 245 Hz were reported (Markwardt et al. 2009, using *RXTE* data), as well as the first type-I X-ray burst (Bozzo et al. 2009, *Swift* data), and burst
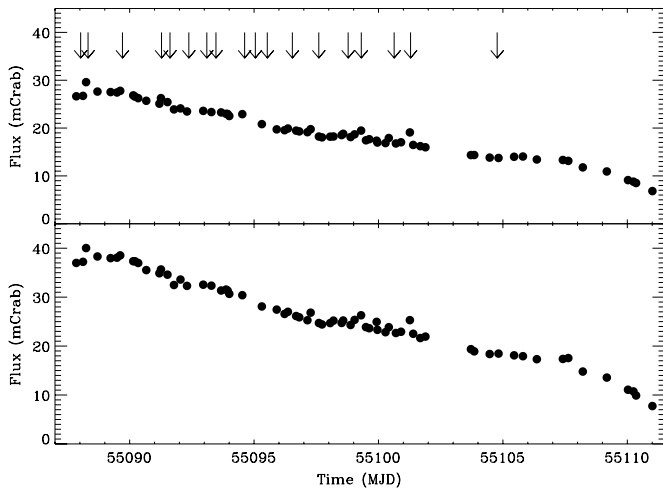
Figure 1. Outburst of IGR J17511−3057 as observed by *RXTE*: 2–10 keV (upper panel) and 10–25 keV (lower panel) intensity, normalized to the Crab. The vertical arrows indicate the times of detected type-I X-ray bursts (Falanga et al. 2011). The *Chandra* data studied here were obtained on 2009 September 22 (MJD 55096).

oscillations very close to the NS spin frequency (Watts et al. 2009, *RXTE* data), making IGR J17511−3057 the fifth LMXB hosting an NS belonging to both the AMXP and NPXP classes.

Similarly to other AMXPs, IGR J17511−3057 can be classified as an atoll source based on its timing and spectral characteristics (Bozzo et al. 2009; Papitto et al. 2010; Kalamkar et al. 2011; Ibragimov et al. 2011; Falanga et al. 2011).

The source faded beyond the *RXTE* detection limit after 2009 October 8 (MJD 55113; Markwardt et al. 2009), with coherent pulsations detected throughout all the outburst. Recently, possible twin kHz quasi-periodic oscillations (QPO) have been reported (Kalamkar et al. 2011). During the whole outburst, a total of 18 type-I X-ray bursts have been detected, marked as vertical arrows in Figure 1: 10 by *RXTE*, 3 by *Swift* (one of which in common with *RXTE*), 2 by *XMM-Newton*, 3 by *INTEGRAL*, and 1 by *Chandra* (see Falanga et al. 2011, for a complete list). With the exception of the *Chandra* one, all the type-I X-ray bursts have been previously studied and reported (Bozzo et al. 2009; Altamirano et al. 2010; Papitto et al. 2010; Falanga et al. 2011; Riggio et al. 2011).

In this paper, we focus on the unpublished *Chandra*/HETG observation of IGR J17511−3057 (2009 September 22, MJD 55096) that we triggered as part of our approved *Chandra* target of opportunity program.

2. THE DATA

We observed IGR J17511−3057 for 20 ks with *Chandra* on 2009 September 22, from 07:40:39 UT until 13:32:03 UT with the High Energy Transmission Grating Spectrometer (Canizares et al. 2000) collecting high-resolution spectral information with the High Energy Grating, HEG 0.8–10 keV, and Medium Energy Grating, MEG 0.4–8.0 keV. The data were analyzed in a standard manner, using the CIAO version 4.3 software package and *Chandra* CALDB version 4.4.6. The spectra were analyzed with the ISIS analysis system, version 1.6.1 (Houck 2002). For pileup correction in the presence of high fluxes (such as the type-I X-ray burst), we used the S-lang script *simple_gpile2*, within the ISIS fitting package, as described in Nowak et al. (2008) and Hanke et al. (2009). The *Chandra* zeroth-order spectrum was not used in the spectral analysis as it severely

suffers from pileup, especially in the burst phase. Given the source brightness and the intrinsic low *Chandra* background, no background removal was applied.

To develop a feeling for the overall flux evolution of IGR J17511−3057, we reduced available *RXTE* data (same dataset of Altamirano et al. 2010). Standard filtering criteria were applied (see, e.g., Rodriguez et al. 2008) and the average count rate was obtained from the top layer of PCU2 for each individual observation. Light curves from the Crab nebula and pulsar from the two closest observations were also extracted and used to renormalize the PCA source count rate to the Crab one.

3. RESULTS

3.1. The X-Ray Position of IGR J17511−3057

We extracted the X-ray position of IGR J17511−3057 from the zeroth-order image obtaining $\alpha_{J2000} = 17^h51^m08^s.66$, $\delta_{J2000} = -30°57'41''.0$, consistent with what we had reported in Nowak et al. (2009).

Figure 2 shows the zeroth-order image at $0''.5$ (upper panel) and $0''.12$ (lower panel) binning (burst plus persistent emission). There is apparent structure in these images due to pileup, especially during the burst portion of the light curve. For this reason, the source location was determined by intersecting the readout streak (visible in the $0''.5$ image) with the grating arms (outside of the field of view covered in the image, but $5''$ wide boxes along the arm positions are shown). This was accomplished with the findzo algorithm, which is standardly used for determining the zeroth-order position when a readout streak is strongly detected (and hence pileup is affecting the zeroth-order image). This is discussed more extensively in Huenemoerder et al. (2011), who discuss its use in the *Chandra* Transmission Gratings Catalog. Its estimated positional uncertainty is $<0''.1$. We note that cross-correlation of Sloan Digital Sky Survey (SDSS) source positions with those obtained from the *Chandra* Source Catalog (CSC)—which relies upon *Chandra* absolute astrometry, as we use here—require only a $0''.16$ 1σ systematic correction (i.e., $0''.26$ at 90% confidence level) to bring the SDSS and CSC positions into statistical agreement. (See Figure 22 of Primini et al. 2011.)

The error we obtain is, however, significantly less than the $0''.6$ 90% confidence level uncertainty claimed for *Chandra* absolute astrometry[6] when no other sources are present in the field of view for refined registration of the field, as is the case for this observation. We, therefore, attribute to the position found a 90% uncertainty of $0''.6$.

3.2. The Type-I Burst Profile

An overview of the outburst of IGR J17511−3057 obtained from *RXTE* data is shown in Figure 1. The *Chandra* data presented here occurred on 2009 September 22 (MJD 55096 in the plot).

A zoom in the light curve of IGR J17511−3057 as obtained during our *Chandra* observation, including the type-I X-ray burst detected at 2009 September 22 12:54:56 UTC, and lasting for about 54 s, is shown in Figure 3. At the time of the burst the source was not being observed by *RXTE*.

Fitting the burst profile with a fast rise exponential decay (hereafter FRED) function, we obtain: a start time of the burst $t_{start} = (17861 \pm 1)$ s, relative to the first photon arrival time of the observation, which translates to 2009 September 22

---

6 http://cxc.harvard.edu/cal/ASPECT/celmon/

Figure 3. Zoom on the type-I X-ray burst observed in our *Chandra* observation of IGR J17511−3057 (2–8 keV). The time is relative to the first photon arrival time of the observation.

(A color version of this figure is available in the online journal.)

3.3. Persistent and Type-I Burst Spectral Analysis

We extracted the spectra of the *persistent* (non-burst) emission as well as of the type-I X-ray burst, hereafter *burst-all*. Furthermore, we divided the burst into three segments that we call hereafter *rise* (about the first 4 s), *peak* (the next 13 s), and *tail* (the next 26 s).[7] These times were chosen also taking into account the more natural CCD-related readout time frame, since the TE mode configuration is not designed to accurately sample fast variability.

For each of the five parts (*persistent*, *burst-all*, *rise*, *peak*, and *tail*), we extracted the first-order dispersed spectra ($m = \pm 1$ for HEG and MEG) and to increase the signal-to-noise ratio, we merged the two HEG ($m = \pm 1$) and MEG ($m = \pm 1$) spectra into one combined spectrum, for a total of five spectra (one per part).[8] Final binning, starting at 0.8 keV, was chosen to have a signal-to-noise ratio higher than 5 and a minimum of 16 MEG channels per bin.

Within the type-I X-ray burst, while we are confident that the *burst-all*, *peak*, and *tail* portions (54, 13, and 26 s, respectively) include no time-tag shift due to the CCDs readout, there may potentially be a problem when integrating something varying as fast as 4 s (*rise*). Hence, though we have extracted its spectrum for visualization purposes, we have decided not to perform spectral fitting of the *rise* bit.

Figure 4 shows four of the five spectra we obtain: *persistent* (black crosses, the dimmest one), *peak* (blue circles, the brightest one), *tail* (brown triangles), and the shortest, 4 s exposure, spectrum of the *rise* with widest energy binning (green squares).

The fit of the *persistent* spectrum with a single non-Comptonized component, be it blackbody or disk blackbody, was very poor, with clear structured residuals. Hence, we used a thermal Comptonization model (nthComp in XSPEC terminology; Zdziarski et al. 1996; Życki et al. 1999), where soft seed photons of temperature kT_s are upscattered by a thermal population of electrons at a temperature of kT_e. Since the hot electrons upscatter the seed photons, there are few photons remaining at energies below the typical seed photon energies, making

---

[7] The final ~10 s of the burst have not been studied separately due to the extremely poor statistics.

[8] The *Chandra* zeroth-order spectrum was not used in the spectral analysis as it severely suffers from pileup, especially in the burst phase.
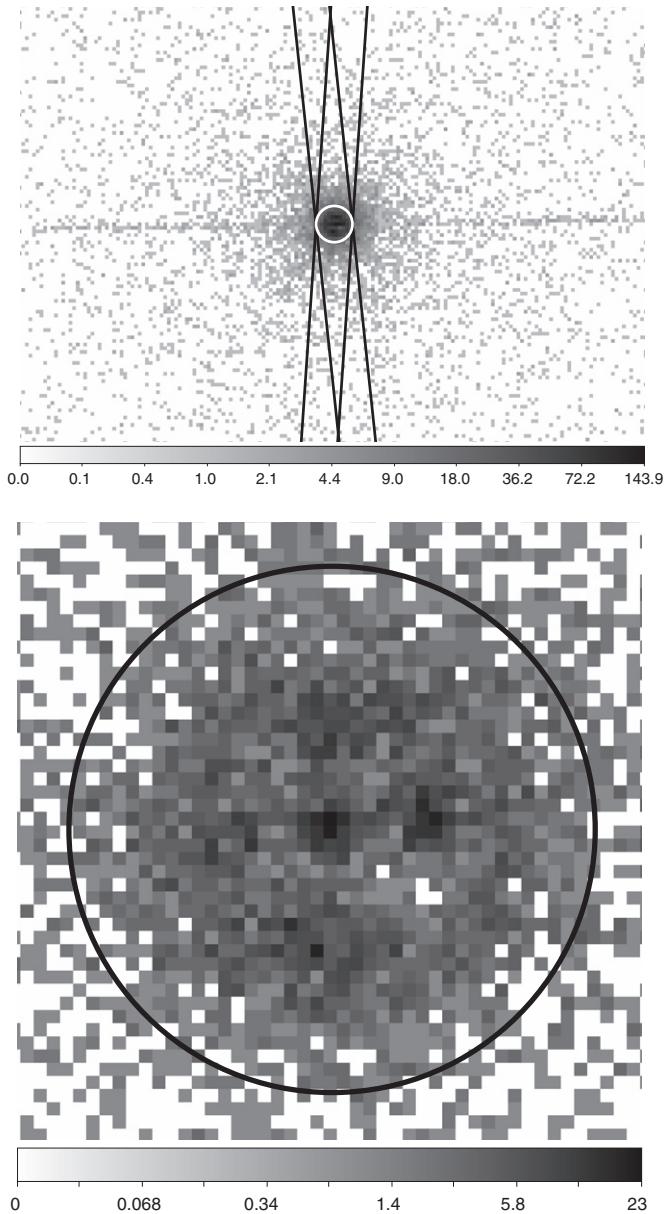
Figure 2. *Chandra* zeroth-order images of IGR J17511−3057. The locations of the zeroth-order and grating arms regions are shown. See the text.

12:54:56 UTC; a rise time of the burst, t_{rise}, within the range of (3.6–6.3) s and a decay time of the burst $t_{\text{decay}} = (14 \pm 1)$ s.

In order to minimize the offset of photon arrival times due to the fact that the CCD chips are read out quasi-serially in the timed exposure (TE) mode, the above results on the FRED properties were obtained using the S3 chip alone. Rectangular regions along the arms (20×90 pixel boxes) and a circular region of 30 pixels around the zeroth order (excising the innermost 16 pixel radius to avoid pileup in the non-dispersed photon region) were used, together with a two-frame bin time, i.e., 3.68 s (1.84 s × 2 frames).

Given the very sharp flux increase of the burst (Figure 3 and $t_{\text{rise}} < 1.2$ s for other reported bursts from the source; Altamirano et al. 2010), it is clear that the binning time used for the fit is likely to affect the result, especially as far as the rise time is concerned. Indeed, a fit with a one-frame bin time (1.84 s) tends to give a shorter rise $t_{\text{rise}} = (1.6–3.6)$ s, but clear residual structures appear, making any attempt to further constrain the rise time inconclusive with the current *Chandra* TE mode.
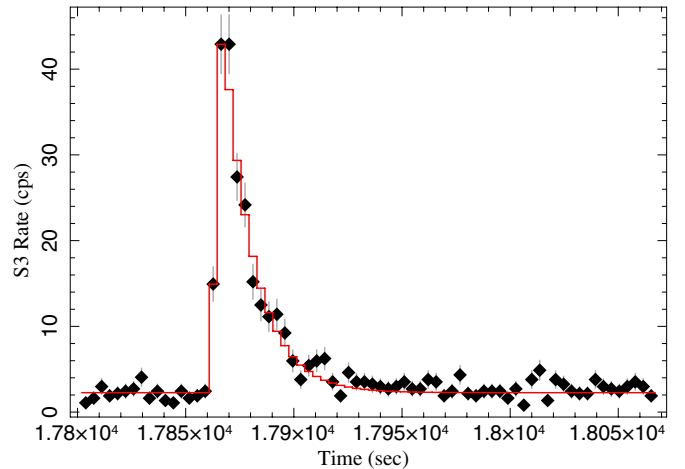
Table 1
Fits to IGR J17511−3057 Spectra: `tbabs*(nthComp +bbodyrad)`

	N_H[a] $(10^{22}\,cm^{-2})$	kT_s (keV)	Γ	kT_e (keV)	kT_{bb} (keV)	R_{bb}[b] (km)	Average Flux[c] $(10^{-10}\,erg\,cm^{-2}\,s^{-1})$	Average Luminosity[d] $(10^{37}\,erg\,s^{-1})$	χ^2/dof
Persistent	1.02 ± 0.05	0.55 ± 0.03	$1.79^{+0.07}_{-0.06}$	[50]	-	-	3.17	0.17	178.2/178
Burst peak (13 s)	[1.02]	[0.55]	[1.79]	[50]	$2.5^{+0.8}_{-0.4}$	5 ± 1	110	5.93	...
Burst tail (26 s)	[1.02]	[0.55]	[1.79]	[50]	$1.3^{+0.2}_{-0.1}$	5.3 ± 0.8	18.9	1.02	...
Burst-all (54 s)	[1.02]	[0.55]	[1.79]	[50]	1.6 ± 0.1	5.2 ± 0.5	28.6	1.6	...

Notes. Errors bars are 90% confidence level for one parameter. The input seed photons to the `nthComp` model are blackbody in shape.
[a] In the fit we have used an improved model for the absorption of X-rays in the interstellar medium by Wilms et al. (2000).
[b] Assuming a distance of 6.9 kpc (Altamirano et al. 2010).
[c] Absorbed 0.5–8 keV flux.
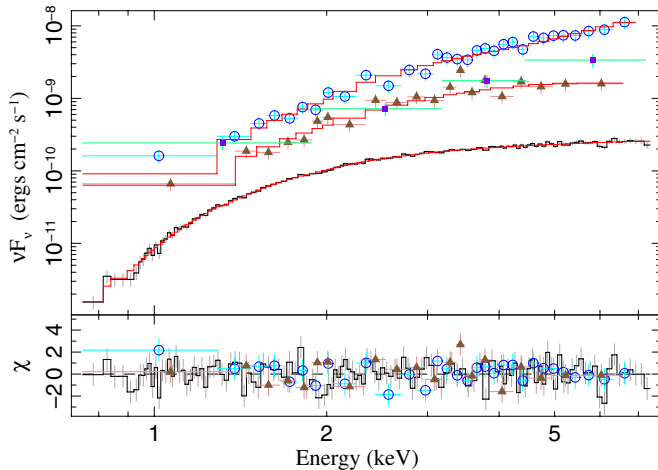[d] Absorbed 0.5–8 keV luminosity, assuming a distance of 6.9 kpc.

Figure 4. Merged HEG ($m = \pm1$) and MEG ($m = \pm1$) spectra for the four extracted segments (see the text): *persistent* (black crosses, the dimmest one), *peak* (blue circles, the brightest one), *tail* (brown triangles), and *rise* with widest energy binning (green).

(A color version of this figure is available in the online journal.)

it significantly different from a power law below this energy. However, the spectrum can be parameterized by an asymptotic power-law index (Γ) that is also a parameter in the model, together with kT_s, kT_e, and the model normalization.

While the low-energy rollover of the spectrum, related to kT_s, can be well appreciated in the *Chandra* energy range, the higher energy one, related to kT_e, is known to be out of the current range (e.g., Papitto et al. 2010). Since our spectral fits are not sensitive to its value, we choose to freeze it to $kT_e = 50\,keV$ in the spectral fit. In the model, the seed photons can be blackbody or disk blackbody but since we cannot discriminate between the two with the current data, we choose to report only the blackbody shape case. Figure 4 shows the best fit we obtained with the absorbed thermal Comptonization model, while Table 1 shows the obtained parameters. In this case, kT_{bb} and R_{bb} of Table 1 are not applicable, since no additional thermal component is required in the *persistent* spectrum (see Section 4.1).

The fits of the *burst-all*, *peak*, and *tail* segments were obtained adding to the above *persistent* model, fixed and considered as the continuum, an additional blackbody component (`bbodyrad` in XSPEC terminology). The obtained best fit, temperatures, and radii (assuming a distance of 6.9 kpc, Altamirano et al. 2010) can also be seen in Table 1.

We note that in all the spectral fitting of Table 1 the additional function *simple_gpile2* was applied to the spectra in order to

correct for pileup distortions, as explained in Nowak et al. (2008) and Hanke et al. (2009).

4. DISCUSSION

4.1. The Persistent Emission

The broadband spectra of AMXPs can normally be described as the composition of an accretion disk emission (peaking below ∼2 keV), a blackbody originating from the hot spot and a hard X-ray emission originated by thermal Comptonization contributing to the whole broadband 1–200 keV emission (e.g., see Figure 1 in Ibragimov et al. 2011, and references therein). As an example of the temperatures involved, the joint *XMM-Newton–RXTE* spectrum of IGR J17511−3057 as observed by Papitto et al. (2010) could be modeled by those three components that were interpreted, from the softest to the hardest, as a multicolored disk emission ($kT_{in} = 0.36 \pm 0.2\,keV$), thermal emission from the NS surface ($kT_{BB} = 0.64^{+0.01}_{-0.02}\,keV$) and thermal Comptonization emission of hotter seed photons ($kT_{seed} = 1.37^{+0.01}_{-0.02}\,keV$) by a hot plasma of electrons ($kT_e = 51^{+6}_{-4}\,keV$, $\tau = 1.34^{+0.03}_{-0.06}$).[9]

In our 20 ks *Chandra* observation, due to lower statistics, the presence of more than one thermal emission component is not required by the data. Indeed, we obtain a single soft population of $kT_s = 0.55 \pm 0.03\,keV$ as seed photons for the Comptonization, most likely the non-disentangled combination of accretion disk and NS surface/halo thermal populations, with no additional thermal component required. A 90% upper limit on the normalization of an additional thermal component, e.g., `bbodyrad` model (with temperature fixed to the Comptonization component of Table 1) gives an absorbed 0.5–8 keV flux of $1.7 \times 10^{-11}\,erg\,cm^{-2}\,s^{-1}$, to be compared with our persistent emission of $3.17 \times 10^{-10}\,erg\,cm^{-2}\,s^{-1}$. This is consistent with what Papitto et al. (2010) obtain using a 70 ks *XMM-Newton* observation,[10] i.e., a total thermal absorbed 0.5–8 keV flux of about $1.3 \times 10^{-11}\,erg\,cm^{-2}\,s^{-1}$, besides the Comptonized `nthComp` component. Furthermore, adding a `diskline` component and freezing its values (except normalization) to the best fit from Papitto et al. (2010, Table 2, *XMM-Newton* data only), we obtain a 90% upper limit on the equivalent width of 50 eV, consistent with that measured by *XMM-Newton*, 43.9 ± 0.06 eV.

The 0.5–8 keV spectrum of IGR J17511−3057 is energetically dominated by a power law which is equivalent to a broader

---

[9] The authors obtain the well constrained Comptonization parameters using simultaneous *XMM-Newton-RXTE* data.
[10] We refer to Table 2 in Papitto et al. (2010), model A, the closest to the one we have here.

Comptonized emission on a limited bandwidth between kT_s and kT_e. In the case of nthComp, the code provides, as the best-fit parameters, the seed photon temperature kT_s, the electron temperature kT_e, and the power-law spectral index Γ.

Since *Chandra* limits us to studying the 0.8–8 keV range, the temperature of the Comptonizing plasma was fixed to $kT_e = 50$ keV, while the photon index of the power law, which dominates the spectrum, was obtained by the fit as $\Gamma = 1.79^{+0.07}_{-0.05}$. Since no high-energy cutoff appears in our *Chandra* spectrum of IGR J17511−3057, the choice of fixing the kT_e parameter to 50 keV does not affect our results. An assumed temperature of, e.g., 100 keV yields comparable results and Γ value.

Once kT_e and Γ are provided, it is possible to infer the Thomson optical depth τ through the relation:

$$\Gamma = \left[\frac{9}{4} + \frac{1}{\left(\frac{kT_e}{m_e c^2}\right)\tau\left(1 + \frac{\tau}{3}\right)} \right]^{1/2} - \frac{1}{2} \qquad (1)$$

(see, e.g., Lightman & Zdziarski 1987). We obtain values of optical depth $\tau = 1$–2 for $kT_e = (50$–100) keV, similarly to that obtained by Papitto et al. (2010).

Using the *persistent* model obtained in Table 1, we obtain $L_{0.5-8\,\mathrm{keV}} = 1.7 \times 10^{36}$ erg s^{-1} (at 6.9 kpc) and an extrapolated unabsorbed $L_{2-200\,\mathrm{keV}} = 7 \times 10^{36}$ erg s^{-1}. This is consistent with Figure 4 in Altamirano et al. (2010), where a persistent $L_{2-200\,\mathrm{keV}} \sim (7$–8) $\times 10^{36}$ erg s^{-1} is expected from the source at 6.9 kpc in the time lasting between the fifth and sixth *RXTE* bursts, when the *Chandra* observation occurred.

A more detailed analysis of the persistent spectrum is not justified by the data. No low-energy features are visible and since the distribution of the residuals does not show any systematic trend, we believe that the best-fit model we obtain (Figure 4 and Table 1) is the simplest and most coherent description of the data, with results compatible with what is found in the literature, albeit subject to uncertainties due to model extrapolations and comparison of different mission calibrations.

4.2. The Type-I Burst

During our *Chandra* observation, a type-I X-ray burst was observed (Figure 3). The burst, fit with a FRED function, resulted in a rise time $t_{rise} = (3.6$–6.3) s (but see Section 3.2) and decay $t_{decay} = (14 \pm 1)$ s. This is "slow" if compared to 10 type-I X-ray bursts of IGR J17511−3057 observed in the *RXTE*/PCA data (Altamirano et al. 2010), where all the bursts reached their maxima within 1.2 s and with decay times in the range of 5–8 s. Although we cannot exclude that this burst is slightly longer than the *RXTE* reported ones, we note that a more accurate comparison is hampered by the limitations of the *Chandra* TE mode, where each chip is exposed for approximately 2 s, to be compared with the 0.1 s time resolution of the *RXTE* data of Altamirano et al. (2010, see Section 3.2).

The low statistics obtained in the burst prevented us from doing an accurate phase-resolved spectroscopy as done in the case of, e.g., the brightest *RXTE* burst (Altamirano et al. 2010; Falanga et al. 2011) or in the *XMM-Newton* ones (Papitto et al. 2010). In our case, it was only possible to split the burst into three segments (*rise*, *peak*, and *tail*), fitting only the latter two because of instrumental limitations (see Section 3.3). As shown in Table 1, the burst emission could be well fit by a single blackbody with the temperature decaying from $kT_{bb} = 2.5^{+0.8}_{-0.4}$ keV to $kT_{bb} = 1.3^{+0.2}_{-0.1}$ keV, likely indicating the cooling of the NS surface after the burst ignition. The related emitting

area has in both cases a radius comparable with ∼5 km that is consistent with that found by, e.g., Falanga et al. (2011) and Papitto et al. (2010) for the other bursts from IGR J17511−3057. We note however that direct comparison with the other X-ray bursts is to be made with caution, because unlike in the other cases, where a detailed phase-resolved analysis was possible, in our study the obtained quantities of Table 1 are averaged over large portions of the burst (e.g., 13 s for the *peak*).

Nevertheless, a comparison of the overall properties of our type-I burst with those previously reported using *RXTE* and *INTEGRAL* can be attempted. Using the *peak* model obtained in Table 1 (with N_H and the nthComp normalization set to 0), we obtain a *peak* unabsorbed luminosity $L_{0.1-40\,\mathrm{keV}} \sim 1.5 \times 10^{38}$ erg s^{-1} for the source at 6.9 kpc. This is a 13 s average value and to compare it with the non-averaged *RXTE* ones, we should estimate our "real peak" value, obtaining it from the FRED function that best fits our burst profile. This results in $L^{peak}_{0.1-40\,\mathrm{keV}} \sim 2.3 \times 10^{38}$ erg s^{-1}, to be compared to Figure 4, middle panel, in Altamirano et al. (2010), where a bolometric peak $L \sim (2.5$–3.5) $\times 10^{38}$ erg s^{-1} is expected from the source at 6.9 kpc, during the *Chandra* observation, between the fifth and sixth *RXTE* bursts.

To obtain an estimate of the overall type-I burst total energy release ($E^{burst}_{0.1-40\,\mathrm{keV}}$) and fluence ($f^{burst}_{0.1-40\,\mathrm{keV}}$), to be compared with the results of the *RXTE* bursts by Altamirano et al. (2010) and of the *RXTE-INTEGRAL* ones by Falanga et al. (2011), we consider the *burst-all* spectrum of Table 1. Setting N_H and the nthComp normalization to 0, we obtain a bolometric unabsorbed luminosity of $L^{burst}_{0.1-40\,\mathrm{keV}} \sim 2 \times 10^{37}$ erg s^{-1} that results in a total energy release of $E^{burst}_{0.1-40\,\mathrm{keV}} \sim 1.1 \times 10^{39}$ erg in 54 s. This is slightly lower than the range obtained by Altamirano et al. (2010), $(2.5$–3) $\times 10^{39}$ erg. Similarly, a fluence of $f^{burst}_{0.1-40\,\mathrm{keV}} = 2 \times 10^{-7}$ erg cm^{-2} is obtained, to be compared to $(3.2$–4.2) $\times 10^{-7}$ erg cm^{-2} of Falanga et al. (2011). In both cases we are dimmer than the previously reported X-ray bursts. Indeed, our burst could be intrinsically dimmer, however considering that we are subject to uncertainties in the model extrapolations beyond the *Chandra* energy domain, as well as to uncertainties in the mission cross-calibrations, it is reasonable to conclude that we have no strong evidence for the type-I X-ray burst observed by *Chandra* from IGR J17511−3057 to be inconsistent with the previously reported bursts. Furthermore, the time-averaging issue reported above and in Section 3.2 due to the TE mode of the observation may be the dominant source of discrepancy. Indeed a limited number of type-I X-ray bursts have been studied up to now with *Chandra* grating; most observations were done in continuous clocking mode (CC), for which the ACIS-S CCDs are read out continuously, providing a ∼3 ms timing, at the expense of one dimension of spatial resolution. An example is, e.g., the study of radius-expansion burst spectra from 4U 1728−34 (Galloway et al. 2010). Out of the 25 bursts detected, time-resolved spectroscopy of the summed signal from the four brightest bursts (with summed bolometric peak flux of about 8×10^{-8} erg cm^{-2} s^{-1}) was carried out. A clear photospheric radius expansion in these bursts could be seen, well sampled over seven time bins on a total of 12 s of burst duration. Stacking data sets from several *Chandra* burst intervals for a more detailed spectral study and evolution has also been the approach of Thompson et al. (2005) for GS 1826−238. Similarly to our case, TE mode had been used and indeed time bins of about 10 s (minimum) were extracted for a spectral study on the six averaged type-I bursts detected from the source (lasting about 150 s).

The *Chandra* observation of IGR J17511−3057 presented here was done in TE mode and a single unexpected 54 s type-I X-ray burst was detected. In this work, we have carefully described our approach to analyzing the light curve and spectra, as the burst is evolving, also showing what can be done within the confines of such an observation.

REFERENCES

Altamirano, D., Casella, P., Patruno, A., Wijnands, R., & van der Klis, M. 2008, ApJ, 674, L45
Altamirano, D., Watts, A., Linares, M., et al. 2010, MNRAS, 409, 1136
Baldovin, C., Kuulkers, E., Ferrigno, C., et al. 2009, ATel, 2196
Bozzo, E., Ferrigno, C., Kuulkers, E., et al. 2009, ATel, 2198
Canizares, C. R., Huenemoerder, D. P., Davis, D. S., et al. 2000, ApJ, 539, L41
Casella, P., Altamirano, D., Patruno, A., Wijnands, R., & van der Klis, M. 2008, ApJ, 674, L41
Falanga, M., Kuiper, L., Poutanen, J., et al. 2011, A&A, 529, A68
Galloway, D. K., Yao, Y., Marshall, H., Misanovic, Z., & Weinberg, N. 2010, ApJ, 724, 417
Hanke, M., Wilms, J., Nowak, M. A., et al. 2009, ApJ, 690, 330
Houck, J. C. 2002, in High Resolution X-ray Spectroscopy with XMM-Newton and Chandra, ed. G. Branduardi-Raymont (London: MSSL), 17
Huenemoerder, D. P., Mitschang, A., Dewey, D., et al. 2011, AJ, 141, 129
Ibragimov, A., Kajava, J. J. E., & Poutanen, J. 2011, MNRAS, 415, 1864
Kaaret, P., Morgan, E. H., Vanderspek, R., & Tomsick, J. A. 2006, ApJ, 638, 963
Kalamkar, M., Altamirano, D., & van der Klis, M. 2011, ApJ, 729, 9
Kuulkers, E., Shaw, S. E., Paizis, A., et al. 2007, A&A, 466, 595
Lightman, A. P., & Zdziarski, A. A. 1987, ApJ, 319, 643
Liu, Q. Z., van Paradijs, J., & van den Heuvel, E. P. J. 2007, A&A, 469, 807
Markwardt, C. B., Altamirano, D., Strohmayer, T. E., & Swank, J. H. 2009, ATel, 2237
Miller-Jones, J. C. A., Russell, D. M., & Migliari, S. 2009, ATel, 2232
Nowak, M. A., Juett, A., Homan, J., et al. 2008, ApJ, 689, 1199
Nowak, M. A., Paizis, A., Wilms, J., et al. 2009, ATel, 2215
Papitto, A., Bozzo, E., Ferrigno, C., et al. 2011, A&A, 535, L4
Papitto, A., Riggio, A., di Salvo, T., et al. 2010, MNRAS, 407, 2575
Patruno, A. 2010, ApJ, 722, 909
Patruno, A., & Watts, A. L. 2012, arXiv:1206.2727
Primini, F. A., Houck, J. C., Davis, J. E., et al. 2011, ApJS, 194, 37
Riggio, A., Papitto, A., Burderi, L., et al. 2011, A&A, 526, A95
Rodriguez, J., Shaw, S. E., Hannikainen, D. C., et al. 2008, ApJ, 675, 1449
Strohmayer, T., & Bildsten, L. 2006, in New Views of Thermonuclear Bursts, ed. W. H. G. Lewin & M. van der Klis (Cambridge Univ. Press), 113
Tauris, T. M., & van den Heuvel, E. P. J. 2006, in Formation and Evolution of Compact Stellar X-ray Sources, ed. W. H. G. Lewin & M. van der Klis (Cambridge Univ. Press), 623
Thompson, T. W. J., Rothschild, R. E., Tomsick, J. A., & Marshall, H. L. 2005, ApJ, 634, 1261
Torres, M. A. P., Jonker, P. G., Steeghs, D., et al. 2009a, ATel, 2233
Torres, M. A. P., Jonker, P. G., Steeghs, D., Simon, J. D., & Gutowski, G. 2009b, ATel, 2216
Watts, A. L., Altamirano, D., Markwardt, C. B., & Strohmayer, T. E. 2009, ATel, 2199
Wilms, J., Allen, A., & McCray, R. 2000, ApJ, 542, 914
Zdziarski, A. A., Johnson, W. N., & Magdziarz, P. 1996, MNRAS, 283, 193
Życki, P. T., Done, C., & Smith, D. A. 1999, MNRAS, 309, 561